Supplement of Atmos. Chem. Phys., 26, 9997–10027, 2026
https://doi.org/10.5194/acp-26-9997-2026-supplement

Atmospheric Chemistry and Physics
Open Access
EGU

Supplement of

Alkaline dust deposition to foliage surfaces likely enhances the dry deposition velocity of SO_2: an investigation in the Alberta Oil-Sands Region using the GEM-MACH air-quality model

Stefan Miller et al.

Correspondence to: Stefan Miller (stefan.miller@ec.gc.ca) and Paul A. Makar (paul.makar@ec.gc.ca)

Contents

S1.0 Further details on the GEM-MACH gas-phase dry deposition algorithms

The formulae for the terms in equation (2) in the main document (aside from r_{ac}, defined in equation (10)) are, respectively (Makar et al., 2018; Clifton et al., 2023),

$$r_m = \frac{1}{\mathrm{LAI}\left(\frac{H^*_{sp}}{3000} + 100 x_{0_{sp}}\right)}, \tag{S1}$$

$$r_s = \frac{r_{s_{min}}}{k_s(Q_p) k_s(\mathrm{VPD}) k_s(T) k_{sc} \mathrm{LAI}} \frac{D_{\mathrm{H_2O}}}{D_{sp}}, \tag{S2}$$

$$r_{cut} = \frac{r_{cut_0}}{\mathrm{LAI}\left(\frac{H^*_{sp}}{10^5} + x_{0_{sp}}\right)}, \tag{S3}$$

$$r_{conv} = 100\left(1 + \frac{1000}{Q_p + 10}\right), \tag{S4}$$

$$r_{exp} = \frac{1}{\frac{H^*_{sp}}{10^5 r_{exp,SO_2}} + \frac{x_{0_{sp}}}{r_{exp,O_3}}}, \tag{S5}$$

and

$$r_g = \frac{1}{\frac{\alpha}{r_{g,SO_2}} + \frac{\beta}{r_{g,O_3}}}. \tag{S6}$$

In these formulae, LAI is the single-sided leaf area index (m^2 leaf area per m^2 ground area), and the relative surface reactivity term x_0 has been parameterized using half-redox potentials outlined in Zhang et al., (2002). Note that the LAI term in Eq. (S1) was inadvertently left out of the corresponding formula in Makar et al., (2018) but has been corrected in subsequent work and herein. In Eq. (S2), $r_{s_{min}}$ is the minimum stomatal resistance. $k_s(Q_p)$, $k_s(\mathrm{VPD})$, $k_s(T)$ and k_{sc} are correction factors (unitless, ranging between 0 and 1) for solar irradiance, the ambient vapor pressure deficit, the air temperature and the atmospheric CO_2 concentration respectively. $\frac{D_{\mathrm{H_2O}}}{D_{sp}}$ is the ratio of the molecular diffusivity of water vapor in air to that of the gas species of interest. The equations describing the correction factors for r_s and $\frac{D_{\mathrm{H_2O}}}{D_{sp}}$ can be found in the supplement of Makar et al., (2018). In Eq. (S3), r_{cut_0} is a constant land-use-specific cuticular resistance for SO_2. In Eq. (S4), Q_p is the solar irradiance incident at the top of the canopy (W m^{-2}). In Eq. (S5) and (S6), $r_{exp,\mathrm{SO_2}}$, r_{exp,O_3}, r_{g,SO_2} and r_{g,O_3} are constant land-use and season specific reference resistances for SO_2 and O_3, with values given in the supplement of Makar et al., (2018).

Wesely's formulations for the cuticle, mesophyll, lower canopy and ground surface resistances all incorporate "parallel" resistance pathways for the removal of gases at each of these depositing surfaces via two chemical processes: (1) dissolution of soluble species (making use of a chemical species-dependent effective Henry's law constant, H^*_{sp}), and (2) reactive destruction at the surface (making use of a chemical species-dependent parameter x_0). Wesely (1989) recognized that most direct observations of gas deposition fluxes are for the gases SO_2 and O_3 – the former being strongly influenced by the surface dissolution pathway, while the latter by the surface reactive destruction pathway. Hence the cuticle, mesophyll, and lower canopy resistance terms make use of ratios of the depositing specie's H^* to that of SO_2, and x_0 is usually expressed to give a relative surface reactivity relative to that of O_3. Thus, in the Wesely formulation of r_c adopted in the GEM-MACH air quality model (Makar et al., 2018), H^*_{sp} is used in the terms describing r_m, r_c and r_{exp} to "scale the rates of uptake by moist and wet surfaces relative to rates for SO_2 uptake" (Wesely, 1989), while the ground resistance term makes use of a two-parameter pair of parallel resistances for SO_2 and O_3 (Zhang

Should be S3, not 5, for the equation number

et al., 2002). This scaling relative to SO_2 is the reason for division of H^*_{sp} by 10^5 in the above formula for r_{cut} and r_{exp}, because for neutral conditions H^*_{sp} for SO_2 ($H^*_{SO_2}$, where $H^*_{SO_2\,neutral} = H^*_{SO_2\,n} \approx 10^5$ M atm^{-1}) and the near-neutral conditions are presumed to be typical of water in plant sap and in the substomatal cavities of the leaves (Wesely, 1989).

Following a multi-model evaluation of ozone deposition algorithms, in which the above GEM-MACH algorithm was found to have a positive bias in the ozone deposition velocity relative to those inferred from ozone flux measurements (Clifton et al., 2023), a re-evaluation of the theoretical basis of the equations was carried out, and two key errors in the original formulation (Makar et al. 2018) were corrected. Equation (5) as above includes an explicit LAI dependence. However, the reference coefficients r_{cut_0} dependant on land-use types and seasons were taken from Zhang et al (2002) wherein the LAI dependence was effectively included in the coefficient formulation. The LAI dependence was thus double counted in Makar et al., (2018) and Clifton et al. (2023), and has been corrected herein with the removal of the explicit LAI term. Thus, Eq. (5) has been removed from the system of equations in the current work and replaced with Eq. (S7):

$$r_{cut_{zha}} = \frac{r_{cut_0}}{\frac{H^*_{sp}}{10^5} + x_{0_{sp}}}. \tag{S7}$$

Similarly, the in-canopy canopy aerodynamic resistance (r_{ac}) term in Makar et al. (2018) and Clifton et al. (2023) was based on Zhang et al. (2003) and only took the reference values (r_{ac_0}) as a function of season and land use only (i.e., values obtained only from a lookup table, that is, $r_{ac} = r_{ac_0}$). However, Zhang et al. (2003) had also included r_{ac} dependencies on the friction velocity (u^*) and LAI, which was neglected in Makar et al., (2018) and Clifton et al. (2023). In this work, these dependencies have been implemented, resulting in a functional expression for r_{ac} as

$$r_{ac} = \frac{r_{ac_0}\,\mathrm{LAI}^{1/4}}{u_*^2}. \tag{S8}$$

The impact of these updates is examined elsewhere in this special issue (Toyota et al., 2026).

Values of H^*_{sp}, x_0, α and β are given in Table S2 for selected gas species. r_{ac_0} and r_{cut_0} as a function of land use type and season are given in Tables S3 and S6 of Makar et al. (2018). The constant values of H^*_{sp} were obtained from Wesley (1989) and Zhang et al., (2002) and are representative of 'neutral conditions' at standard temperature and pressure. x_0, α and β were obtained from the supplement of Makar et al., (2018) and Zhang et al., (2002). In this work, H^*_{sp} is allowed to vary with the predicted $[H^+]$ concentration in the leaf water solution (see Sect. 2.2) and the air temperature (T with units K). The formulae describing the $[H^+]$ dependence on H^* for some gas species are given in Table S1. Effective Henry's Law constants H^*_{sp} are different from the intrinsic Henry's law constants H_{sp} in that they can include the effects of ionic dissociation of the dissolving gas into multiple stages of ions within solution, which may increase the partitioning to the aqueous phase.

Table S1: Values of H^*_{sp} and x_0 for some common gaseous species. Tabulated data for H^*_{sp} are from Wesley (1989) and Zhang et al., (2002).
x_0, α and β are from Zhang et al., (2002) and Makar et al., (2018). The formula describing $H^*_{SO_2}$ and $H^*_{NH_3}$ were obtained from Chameides (1984) and Shi et al., (1999) respectively. The remaining H^* formulae are from Evrens et al. (2003).

Gaseous species (sp)	Chemical formula	H^*_{sp} (M atm^{-1}) (Wesley, 1989)	H^*_{sp} (M atm^{-1})	x_0	α	β
Sulphur dioxide	SO_2	10^5	$H^*_{SO_2} = 1.23\exp\left[3120\left(\frac{1}{T}-\frac{1}{298}\right)\right]\left(1+\frac{K_{EQ_1}}{[H^+]}+\frac{K_{EQ_1}K_{EQ_2}}{[H^+]^2}\right)$, where $K_{EQ_1} = 1.7\times10^{-2}\exp\left[2090\left(\frac{1}{T}-\frac{1}{298}\right)\right]$, and $K_{EQ_2} = 6\times10^{-8}\exp\left[1120\left(\frac{1}{T}-\frac{1}{298}\right)\right]$	0	1	0
Ozone	O_3	0.01	$H^*_{O_3} = H_{O_3} = 1.42\times10^{-2}\exp\left[2800\left(\frac{1}{T}-\frac{1}{298.15}\right)\right]$	1	0	1
Nitrogen dioxide	NO_2	0.01	$H^*_{NO_2} = H_{NO_2} = 1.0\times10^{-2}$	0.1	0	0.8
Nitric oxide	NO	2×10^{-3}	$H^*_{NO} = H_{NO} = 1.93\times10^{-3}\exp\left[1600\left(\frac{1}{T}-\frac{1}{298.15}\right)\right]$	0	0	0.01
Nitric acid	HNO_3	10^{14}	$H^*_{HNO_3} = 2.1\times10^5\exp\left[8700\left(\frac{1}{T}-\frac{1}{298.15}\right)\right]\left[\frac{1+22\exp\left[1800\left(\frac{1}{T}-\frac{1}{298.15}\right)\right]}{[H^+]}\right]$	0	10	10
Hydrogen peroxide	H_2O_2	10^5	$H^*_{H_2O_2} = H_{H_2O_2} = 1.42\times10^5\exp\left[6300\left(\frac{1}{T}-\frac{1}{298.15}\right)\right]$	1	1	1
Ammonia	NH_3	2×10^4	$H^*_{NH_3} = H_{NH_3}\left(1+\frac{K_{NH_4^+}}{K_w}[H^+]\right)$, $H_{NH_3} = 59.8\exp\left[4200\left(\frac{1}{T}-\frac{1}{298.15}\right)\right]$ [M atm^{-1}], $K_{NH_4^+} = \exp\left(16.97-\frac{4411.1}{T}-0.044T\right)$ [M], $K_w = \exp\left(-23.6+\frac{1550.1}{T}-\frac{1.229\times10^6}{T^2}\right)$ [M^2]	0	1	0
Nitrous acid	HONO	10^5	$H^*_{HONO} = 48.6\exp\left[4800\left(\frac{1}{T}-\frac{1}{298.15}\right)\right]\left[\frac{1+5.3\times10^{-4}\exp\left[-1760\left(\frac{1}{T}-\frac{1}{298.15}\right)\right]}{[H^+]}\right]$	0.1	2	2

S2.0 Mathematical details on the modification to the gas-phase deposition algorithm to account for cuticle fluxes

Noting that (1) the pH dependence will act only on the cuticle resistance and (2) the pH dependence will only be applied to a subset of land-use types (the "natural" land use types in the main text), we define f_i as the grid-cell specific land-use type fraction for the ith land use type of the $nlus$ land use types in the model, and a parameter δ_i, where $\delta_i = 1$ when the land-use type is one in which the pH dependence is to be calculated, and $\delta_i = 0$ otherwise. The deposition velocity of the *j*'th gas for the *i*'th land use type can be expressed as:

$$V_{d\,j} = \sum_{i=1}^{nlus}(v_{d\,j,i}\times f_i) = \sum_{i=1}^{nlus}(v_{d\,j,i}\times f_i\times\delta_i) + \sum_{i=1}^{nlus}(v_{d\,j,i}\times f_i\times[1-\delta_i]) \quad \text{(S9)}$$

The fraction of the deposition velocity for *j*'th gas and the *i*'th land use type which can be attributed to cuticle resistance is given by the effective conductance formula (Galmarini et al., 2021; Clifton et al., 2023):

$$E_{j,i} = \frac{\frac{1}{r_{cut\,j,i}}}{\frac{1-W_{st}}{r_{sj,i}+r_{m\,j,i}}+\frac{1}{r_{cut\,j,i}}+\frac{1}{r_{exp\,j,i}+r_{conv\,j,i}}+\frac{1}{r_{ac\,j,i}+r_{g\,j,i}}} \quad \text{(S10)}$$

(S10) may be substituted back into the natural land use type summation (first of the two summation) of (S9), splitting that term into cuticle and non-cuticle contributions to the natural land use type contributions to deposition velocity:

$$V_{d\,j} = \sum_{i=1}^{nlus}\left(v_{d\,j,i} \times f_i \times \delta_i \times E_{j,i}\right) + \sum_{i=1}^{nlus}\left(v_{d\,j,i} \times f_i \times \delta_i \times \left(1 - E_{j,i}\right)\right) + \sum_{i=1}^{nlus}(v_{d\,j,i} \times f_i \times [1 - \delta_i]) \quad \text{(S11)}$$

The fraction of the deposition velocity for the *j*'th gas associated with the cuticle resistance for natural vegetation is thus the ratio of the first term of (S11) to the total deposition velocity is thus given by:

$$\alpha_{cut_j} = \frac{\sum_{i=1}^{nlus}(v_{d\,j,i} \times f_i \times \delta_i \times E_{j,i})}{\sum_{i=1}^{nlus}(v_{d\,j,i} \times f_i)} \quad \text{(S12)}$$

The proportion of the net deposition flux for the *j*'th gas which can be attributed to the cuticle resistance (a quantity known as the cuticle effective flux; Galmarini et al., 2021) can be expressed using the gas concentration C_j (moles m^{-3})

$$F_{cut_j} = \alpha_{cut\,j} \times V_{d\,j} \times C_j \times \Delta t = \alpha_{cut\,j} \times F_j \quad \text{(S13)}$$

Thus, to calculate the cuticle portion of the net deposition flux (F_j) for most gases *j*, the only additional quantity which must be calculated in addition to the flux is the value of $\alpha_{cut\,j}$, from equation (S12).

Ammonia gas (NH_3) must be considered as a special case,; in GEM-MACH a bi-directional flux algorithm is applied to NH_3 (Zhang et al., 2010, see Figure S1 for the corresponding deposition resistance diagram), wherein the leaf cuticle is always a sink and hence the calculation $F_{cut_{\mathrm{NH_3}}}$ (mol m^{-2}) becomes

$$F_{cut_{\mathrm{NH_3}}} = V_{d\,cut_{\mathrm{NH_3}}} \times C_{\mathrm{NH_3}}^{canopy\_top} \times \Delta t \quad \text{(S14)}$$

where

$$V_{d\,cut_{\mathrm{NH_3}}} = \frac{1}{r_{cut_{NH_3}}} \text{ and} \quad \text{(S15)}$$

$$C_{\mathrm{NH_3}}^{canopy\_top} = \frac{x_{c_{\mathrm{NH_3}}} \times 10^{-6}}{M_{\mathrm{NH_3}}}. \quad \text{(S16)}$$

$V_{d\,cut_{\mathrm{NH_3}}}$ is the dry deposition velocity of NH_3 to the leaf cuticle (m s^{-1}), Δt is the model timestep with units of s, $x_{c_{\mathrm{NH_3}}}$ is a vegetation-and-meteorology-dependent canopy compensation point concentration of NH_3 (μg m^{-3}, or the concentration of NH_3 at the canopy top), $M_{\mathrm{NH_3}}$ = 17.031 g mol^{-1} is the molecular mass of NH_3 and the 10^{-6} factor is applied to convert from μg to g. In the Zhang et al., (2010) bidirectional NH_3 flux parameterization applied herein, the resulting deposition velocity $V_{d\,cut_{\mathrm{NH_3}}}$ does not depend on H^*. Instead, r_{cut} for NH_3 is determined from Eq. (9) presented in Zhang et al., (2003), where the LAI, relative humidity, and friction velocity (u_*) are used as factors to dynamically adjust a constant value of r_{cut_0} value ascribed to different land use types and to meteorological conditions (i.e., rain vs. dew vs. dry).

S3.0 Mathematical details on the modification to the particle deposition algorithm to account for cuticle fluxes

For a particle of median size index k, the deposition velocity in GEM-MACH for land-use type i is calculated as (Zhang et al., 2001; Emerson et al., 2020)

$$v_{d\,i,k} = v_{s_k} + \frac{1}{r_{a_i} + r_{c\,i,k}} \quad \text{(S17)}$$

where v_{s_k} is the size-dependant settling velocity of the particles of median size *k*, and r_{a_i} is the aerodynamic resistance. $r_{c_{i,k}}$ is the canopy resistance for particles of median size *k*, and is calculated in GEM-MACH as (Zhang et al., 2001; Emerson et al., 2020),

$$r_{c_{i,k}} = \frac{1}{\alpha_0 u_* \varepsilon_{i,k}} \quad \text{(S18)}$$

where α_0 is set to a constant value of 3.0. GEM-MACH resolves size-dependant particle deposition across 12 size bins (index n_{size}). Hence, for each grid cell the fraction of the deposition velocity that is to a natural vegetative land use type for particle size range k is calculated as

$$E_{\mathrm{p}_k} = \frac{\sum_{i=1}^{nlus}\left[\delta_i \times f_i \times v_{d_{i,k}}\right]}{\sum_{i=1}^{nlus}\left[f_i \times v_{d_{i,k}}\right]} \quad \text{(S19)}$$

We can then define the flux of a particle species *sp* within the internally-mixed particle of size *k* across all vegetation types in a grid cell and its fraction entering the natural land-use types as $F_{sp,k}$ and $\eta_{veg_{\mathrm{p}sp}}$ respectively,

$$\eta_{veg_{sp}} = \frac{\sum_{k=1}^{n_{size}}\left(E_{\mathrm{p}_k} \times F_{sp,k}\right)}{\sum_{k=1}^{n_{size}}\left(F_{sp,k}\right)} = \frac{\sum_{k=1}^{n_{size}}\left(E_{\mathrm{p}_k} \times F_{sp,k}\right)}{F_{sp}}, \quad \text{(S20)}$$

where F_{sp} is the total mass flux of the particle species *sp* across all sizes within the grid cell. Finally, the calculation of the total deposition flux for the particle species *sp* in the grid cell to the leaf cuticle pathway requires the introduction of the partitioning factor ($\alpha_{cut_{\mathrm{sp}}}$) as

$$F_{cut_{sp}} = \alpha_{cut_{\mathrm{sp}}} \times \eta_{veg_{sp}} \times F_{\mathrm{sp}} \quad \text{(S21)}$$

$\alpha_{cut_{sp}}$ represents the fraction of $\eta_{veg_{sp}}$ due to deposition to the leaf surface (as opposed to deposition to bark or the ground beneath the canopy). Since our dry deposition parameterization for aerosol particles (S17) is not built upon attributions of the individual pathways of deposition, $\alpha_{cut_{sp}}$ must be estimated using surrogate information. Here, we have assumed that the total area available for deposition of particles is the sum of the leaf area in the vertical column through the canopy (i.e. the leaf area index, LAI) plus the surface area of the ground below the leaves. A first approximation to $\alpha_{cut_{sp}}$ is thus given by:

$$\alpha_{cut_{\mathrm{p}sp}} = \frac{\mathrm{LAI}}{\mathrm{LAI} + 1.0}. \quad \text{(S22)}$$

Eq. (S22) is strictly a function of the LAI but could be modified if additional data became available (for example, the relative amount of surface area available for deposition in the vertical column which is composed of twigs, branches, etc). Any additional terms added to Eq. (S22) would likely appear in the denominator, hence the value of $F_{cut_{sp}}$ calculated using Eq. (S22) and should probably be taken as an upper limiting value.

S4.0 Theoretical Development and Description of the Carbonate Adjustment Module CALCCO3

Table S2: Chemical species in gas, aqueous and solid phases and their thermodynamic properties assumed in CALCCO3 (Fountoukis & Nenes 2007; Meng et al., 1995).

Species	ΔG° (kJ mol^{-1})	ΔH° (kJ mol^{-1})	C_p° (J mol^{-1} K^{-1})
$NH_3(aq)$	-26.500	-80.290	79.900
$NH_4^+(aq)$	-79.310	-132.510	79.900
$H^+(aq)$	0.000	0.000	0.000
$OH^-(aq)$	-157.244	-229.994	-148.500
$HSO_4^-(aq)$	-755.910	-887.340	-84.000
$SO_4^{2-}(aq)$	-744.530	-909.270	-293.000
$CO_2(g)$	-394.359	-393.509	37.11
$CO_2(aq)$	-385.980	-413.80	277.64
$Na_2CO_3(s)$	-1044.44	-1130.68	112.30
$K_2CO_3(s)$	-1063.5	-1151.02	114.43
$CaCO_3(s)$	-1128.79	-1206.92	81.88
$MgCO_3(s)$	-1012.1	-1095.8	75.52
$HCO_3^-(aq)$	-586.77	-691.99	88.43
$CO_3^{2-}(aq)$	-527.81	-677.14	-234.52
$Mg^{2+}(aq)$	-454.800	-466.850	-
$Ca^{2+}(aq)$	-553.580	-542.830	-
$K^+(aq)$	-283.270	-252.830	21.800
$Na^+(aq)$	-261.905	-240.120	46.400

The equilibrium constants for reversible reactions vary with temperature according to the van't Hoff equation:

$$K(T) = \exp\left(-\frac{\Delta G^\circ}{RT_0}\right)\exp\left[-\frac{\Delta H^\circ(T_0)}{RT_0}\left(\frac{T_0}{T}-1\right)-\frac{\Delta C_p^\circ}{R}\left(1+\ln\left(\frac{T_0}{T}\right)-\frac{T_0}{T}\right)\right] \quad \text{(S23)}$$

Where

$$K_0 = \exp\left(-\frac{\Delta G^\circ}{RT_0}\right),\ H_0 = \frac{\Delta H^\circ(T_0)}{RT_0} \text{ and } C_{p_0} = \frac{\Delta C_p^\circ}{R},\ T_0 = 298.15 \text{ K},\ R = 8.3145 \text{ J mol}^{-1} \text{ K}^{-1} \quad \text{(S24)}$$

ΔG°, ΔH° and ΔC_p° represent the Gibbs free energy, enthalpy and specific heat a constant pressure respectively, due to reactions from the lefthand side to righthand side of the reversible reaction formulae (Table S2). They are derived from thermodynamic properties of the species involved in the reactions (Table S1). For example, for the equilibrium reaction $NH_4^+ \leftrightarrow H^+ + NH_3(aq)$:

$\Delta G^\circ = \Delta_f G^\circ_{NH_3} + \Delta_f G^\circ_{H^+} - \Delta_f G^\circ_{NH_4^+} = -26.500 + 0.000 - (-79.310) = 52.810$ kJ mol^{-1},

$\Delta H^\circ = \Delta_f H^\circ_{NH_3} + \Delta_f H^\circ_{H^+} - \Delta_f H^\circ_{NH_4^+} = -80.290 + 0.000 - (-132.510) = 52.220$ kJ mol^{-1} and

$\Delta C_p^\circ = \Delta C^\circ_{p_{NH_3}} + \Delta C^\circ_{p_{H^+}} - \Delta C^\circ_{p_{NH_4^+}} = -79.900 + 0.000 - (-79.900) = 0.0$ J mol^{-1} K^{-1}.

Table S3: Reversible chemical reactions and their equilibrium constants (K_0) at a standard temperature of 298.15 K, and parameters H_0 and C_{p_0} describing the temperature dependence considered in CALCCO3.

Equilibrium Reaction	Equilibrium Expression	K_0	H_0	C_{p_0}	Units
$H_2O \leftrightarrow H^+ + OH^-$	$K_w = [H^+][OH^-]$	1.01×10^{-14}	-22.52	26.92	mol^2 kg^{-2}
$HSO_4^- \leftrightarrow H^+ + SO_4^{2-}$	$K_{HSO_4} = \frac{[H^+][SO_4^{2-}]}{[HSO_4^-]}$	1.015×10^{-2}	8.85	25.14	mol kg^{-1}
$NH_4^+ \leftrightarrow H^+ + NH_3(aq)$	$K_{NH_4} = \frac{[NH_3]_{(aq)}[H^+]}{[NH_4^+]}$	5.599×10^{-10}	21.07	0.00	mol kg^{-1}
$CO_2(g) \leftrightarrow CO_2(aq)$	$K_{CO_2} = \frac{[CO_2(aq)]}{p_{CO_2}}$	3.404×10^{-2}	-8.1858	28.9307	mol kg^{-1} atm^{-1}
$CO_2(aq) + H_2O \leftrightarrow H^+ + HCO_3^-$	$K_{HCO_3} = \frac{[HCO_3^-][H^+]}{[CO_2(aq)]}$	4.299×10^{-7}	3.0821	-31.8139	mol kg^{-1}
$HCO_3^- \leftrightarrow H^+ + CO_3^{2-}$	$K_{CO_3} = \frac{[CO_3^{2-}][H^+]}{[HCO_3^-]}$	4.678×10^{-11}	5.9908	-38.8440	mol kg^{-1}
$CaCO_3(s) \leftrightarrow Ca^{2+} + CO_3^{2-}$	$K_{CaCO_3} = [Ca^{2+}][CO_3^{2-}]$	4.959×10^{-9}	-	-	mol^2 kg^{-2}
$MgCO_3(s) \leftrightarrow Mg^{2+} + CO_3^{2-}$	$K_{MgCO_3} = [Mg^{2+}][CO_3^{2-}]$	6.812×10^{-6}	-	-	mol^2 kg^{-2}
$K_2CO_3 \leftrightarrow 2K^+ + CO_3^{2-}$	$K_{K_2CO_3} = [K^+]^2[CO_3^{2-}]$	2.541×10^5	-12.4575	-36.7272	mol^3 kg^{-3}
$Na_2CO_3 \leftrightarrow 2Na^+ + CO_3^{2-}$	$K_{Na_2CO_3} = [Na^+]^2[CO_3^{2-}]$	18.11	-10.7713	-30.5533	mol^3 kg^{-3}

This should be S3

Model inputs to CALCCO3 are concentrations C (except water) in units of mol m^{-3} air and the liquid water content denoted L_w in units of kg m^{-3}, whereas equilibrium expressions in Table S2 require concentrations (X) to have units of mol kg^{-1} (i.e., molalities, where the solvent here is water). Thus, the inputs are converted as follows:

$$X\left(\frac{\text{mol}}{\text{kg}}\right) = \frac{C\left(\frac{\text{mol}}{\text{m}^3}\right)}{L_w\left(\frac{\text{kg}}{\text{m}^3}\right)} \quad \text{(S25)}$$

CALCCO3 solves the electroneutrality equation iteratively using the bisection method, where the bisected variable is $[H^+]_B$. All concentrations are in mol kg^{-1} water and partial pressures are in atm. Equilibrium constants follow the same units as the species in their expressions (see Table S2). The electroneutrality equation is

$$[H^+]_B + [NH_4^+] + 2[Ca^{2+}] + 2[Mg^{2+}] + [K^+] + [Na^+] = [OH^-] + [HSO_4^-] + 2[SO_4^{2-}] + [Cl^-] + [NO_3^-] + [HCO_3^-] + 2[CO_3^{2-}] \quad \text{(S26)}$$

The initial aqueous speciation used as inputs for CALCCO3 are obtained from HETP, where

$$TS = [SO_4^{2-}] + [HSO_4^-] \quad \text{(S27)}$$

$$TA = [NH_4^+] + [NH_3]_{(aq)} \quad \text{(S28)}$$

$$TCl = [Cl^-] \quad \text{(S29)}$$

$$TN = [NO_3^-], \quad \text{(S30)}$$

and initially $[NH_3]_{(aq)} = 0$. HETP assigns part of base cations to protons being associated with strong acid and base anions, other than HCO_3^- and CO_3^{2-}, denoted here by a subscript i. Any remaining free (excess) base cations that are not assigned with an anion (i.e., T_{MgCO_3}, T_{CaCO_3}, $T_{K_2CO_3}$, $T_{Ca_2CO_3}$) are assumed to be matched by carbonate (CO_3^{2-}). These enter CALCCO3 initially as solid carbonates magnesium carbonate, calcium carbonate, potassium carbonate and sodium carbonate, represented below by T_{MgCO_3}, T_{CaCO_3}, $T_{K_2CO_3}$, $T_{Na_2CO_3}$ respectively. The total magnesium, total calcium, total potassium and total sodium are, respectively,

$$TMg = [Mg^{2+}]_i + T_{MgCO_3} \quad \text{(S31)}$$

The Mg in TMg should be as a subscript, similar to TK and TNa in Eqns S33 and S334

The Ca in TCa should be as a subscript, similar to TK and TNa in equations S33 and S34.

$$TCa = [Ca^{2+}]_i + T_{CaCO_3} \quad (S32)$$

$$T_K = [K^+]_i + T_{K_2CO_3} \quad (S33)$$

$$T_{Na} = [Na^+]_i + T_{Na_2CO_3} \quad (S34)$$

The following expressions are used reduce the number of unknown variables in Eq. (S26). For hydroxide (OH^-), we use

$$[OH^-] = \frac{K_w}{[H^+]} \quad (S35)$$

From Eq. (S27), $TS - [HSO_4^-] = [SO_4^{2-}]$, hence

$$K_{HSO_4} = \frac{[H^+][SO_4^{2-}]}{[HSO_4^-]} = \frac{[H^+](TS-[HSO_4^-])}{[HSO_4^-]} \quad (S36)$$

which can be rearranged to

$$[HSO_4^-] = \frac{TS}{1+\frac{K_{HSO_4}}{[H^+]}} \quad (S37)$$

$$[SO_4^{2-}] = TS - [HSO_4^-]. \quad (S38)$$

Should be "from", not "form"

Similarly form equation (S28), $TA - [NH_4^+] = [NH_3]_{(aq)}$, hence

$$K_{NH_4} = \frac{[NH_3]_{(aq)}[H^+]}{[NH_4^+]} = \frac{[H^+](TA-[NH_4^+])}{[NH_4^+]} \quad (S39)$$

which can be rearranged to

$$[NH_4^+] = \frac{TA}{1+\frac{K_{NH_4}}{[H^+]}}. \quad (S40)$$

$$[NH_3]_{(aq)} = TA - [NH_4^+] \quad (S41)$$

Please subscript the "2" in "CO2".

Next, we define the total dissolved inorganic carbon (TC) as

$$TC = [CO_2(aq)] + [HCO_3^-] + [CO_3^{2-}] \quad (S42)$$

where we assume initially that $CO_{2_{aq}}$ is in equilibrium with the gas-phase CO2 via dissolution or volatilization, so

$$K_{CO_2} = \frac{[CO_2(aq)]}{p_{CO_2}} \quad (S43)$$

hence

$$[CO_2(aq)] = K_{CO_2} p_{CO_2}. \quad (S44)$$

And $[HCO_3^-]$ and $[CO_3^{2-}]$ follow

$$K_{HCO_3} = \frac{[HCO_3^-][H^+]}{[CO_2(aq)]} \quad (S45)$$

hence

$$[HCO_3^-] = \frac{K_{HCO_3}[CO_2(aq)]}{[H^+]}, \quad (S46)$$

and

$$K_{CO_3} = \frac{[CO_3^{2-}][H^+]}{[HCO_3^-]} \quad (S47)$$

hence

Could a space be inserted between TC and KCO3 in eq S51? Hard to make out that they are separate variables, the way they look here.

$$[CO_3^{2-}] = \frac{K_{CO_3}[HCO_3^-]}{[H^+]} = \frac{K_{CO_3}K_{HCO_3}[CO_2(aq)]}{[H^+]^2} \quad (S48)$$

By using Eq. (S46) and Eq. (S48), TC can be rewritten as a function of $[CO_2(aq)]$ and $[H^+]$:

$$TC = [CO_2(aq)]\left(1 + \frac{K_{HCO_3}}{[H^+]} + \frac{K_{CO_3}K_{HCO_3}}{[H^+]^2}\right) \quad (S49)$$

By using a relation between TC and $[CO_2(aq)]$ from Eq. (S49), Eq. (S46) can be rewritten to represent a relation between TC and $[HCO_3^-]$

$$[HCO_3^-] = \frac{TCK_{HCO_3}[H^+]}{[H^+]^2+[H^+]K_{HCO_3}+K_{CO_3}K_{HCO_3}}. \quad (S50)$$

Similarly, by combining Eq. (S48) and Eq. (S49), we obtain

$$[CO_3^{2-}] = \frac{TCK_{CO_3}K_{HCO_3}}{[H^+]^2+[H^+]K_{HCO_3}+K_{CO_3}K_{HCO_3}}. \quad (S51)$$

Solubility-limited, stepwise solid carbonate dissolution is then assumed, and applied according to

$$[Ca^{2+}]_d = \min\left(T_{CaCO_3}, \frac{K_{CaCO_3}}{[CO_3^{2-}]}\right) \quad (S52)$$

where $[CO_3^{2-}]$ is calculated from Eq. (S51), and $TC = TC + [Ca^{2+}]_d$ since additional $[CO_3^{2-}]$ has been added through dissolution. Following this, $[CO_3^{2-}]$ is then recalculated from Eq. (S51) and $MgCO_3$ dissolution is performed according to

$$[Mg^{2+}]_d = \min\left(T_{MgCO_3}, \frac{K_{MgCO_3}}{[CO_3^{2-}]}\right). \quad (S53)$$

Once again, TC is updated as $TC = TC + [Mg^{2+}]_d$. Thereafter, K_2CO_3 and Na_2CO_3 dissolution is performed as

$$[K^+]_d = \min\left(T_{K_2CO_3}, 2\left[\frac{K_{K_2CO_3}}{4}\right]^{1/3}\right) \quad (S54)$$

and

$$[Na^+]_d = \min\left(T_{Na_2CO_3}, 2\left[\frac{K_{Na_2CO_3}}{4}\right]^{1/3}\right) \quad (S55)$$

and TC is updated to $TC = TC + [K^+]_d + [Na^+]_d$. Using the final updated TC, a final $[CO_3^{2-}]$ is recalculated from Eq. (S51). Subsequently, a final $[HCO_3^-]$ is calculated from Eq. (S50). Finally, base cations are calculated from

$$[Ca^{2+}] = [Ca^{2+}]_i + [Ca^{2+}]_d \quad (S56)$$

$$[Mg^{2+}] = [Mg^{2+}]_i + [Mg^{2+}]_d \quad (S57)$$

$$[K^+] = [K^+]_i + 2[K^+]_d \quad (S58)$$

$$[Na^+] = [Na^+]_i + 2[Na^+]_d. \quad (S59)$$

Thus, (S29), (S30), (S35), (S37), (S38), (S40), (S50), (S51), (S56), (S57), (S58) and (S59) fully define all ion speciation required to solve (S26) as an electroneutrality error δ_E

$$\delta_E = [H^+]_B + [NH_4^+] + 2[Ca^+] + 2[Mg^{2+}] + [K^+] + [Na^+] - ([OH^-] + [HSO_4^-] + 2[SO_4^{2-}] + [Cl^-] + [NO_3^-] + [HCO_3^-] + 2[CO_3^{2-}]). \quad (S60)$$

Once $\delta_E < 1 \times 10^{-12}$ convergence is achieved, and pH is derived from a final $[H^+]_B$ calculated from Eq. (S60).

S5.0 Additional figures and tables

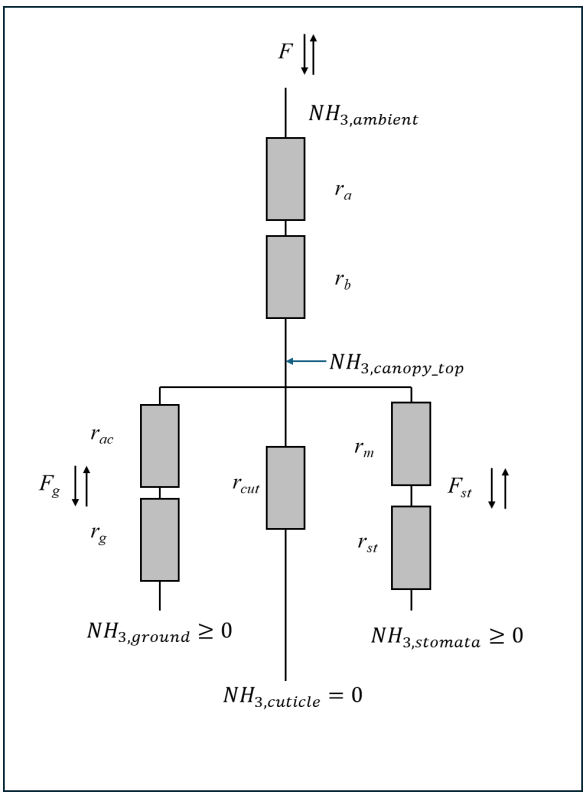

Figure S1: NH_3 bidirectional flux resistances (after Zhang et al., 2010).

Note that the deposition flux via the cuticle pathway depends on the concentration of NH_3 at the top of the canopy; this is referred to as $\boldsymbol{C}_{\mathbf{NH_3}}^{\boldsymbol{canopy\_top}}$ in the text.

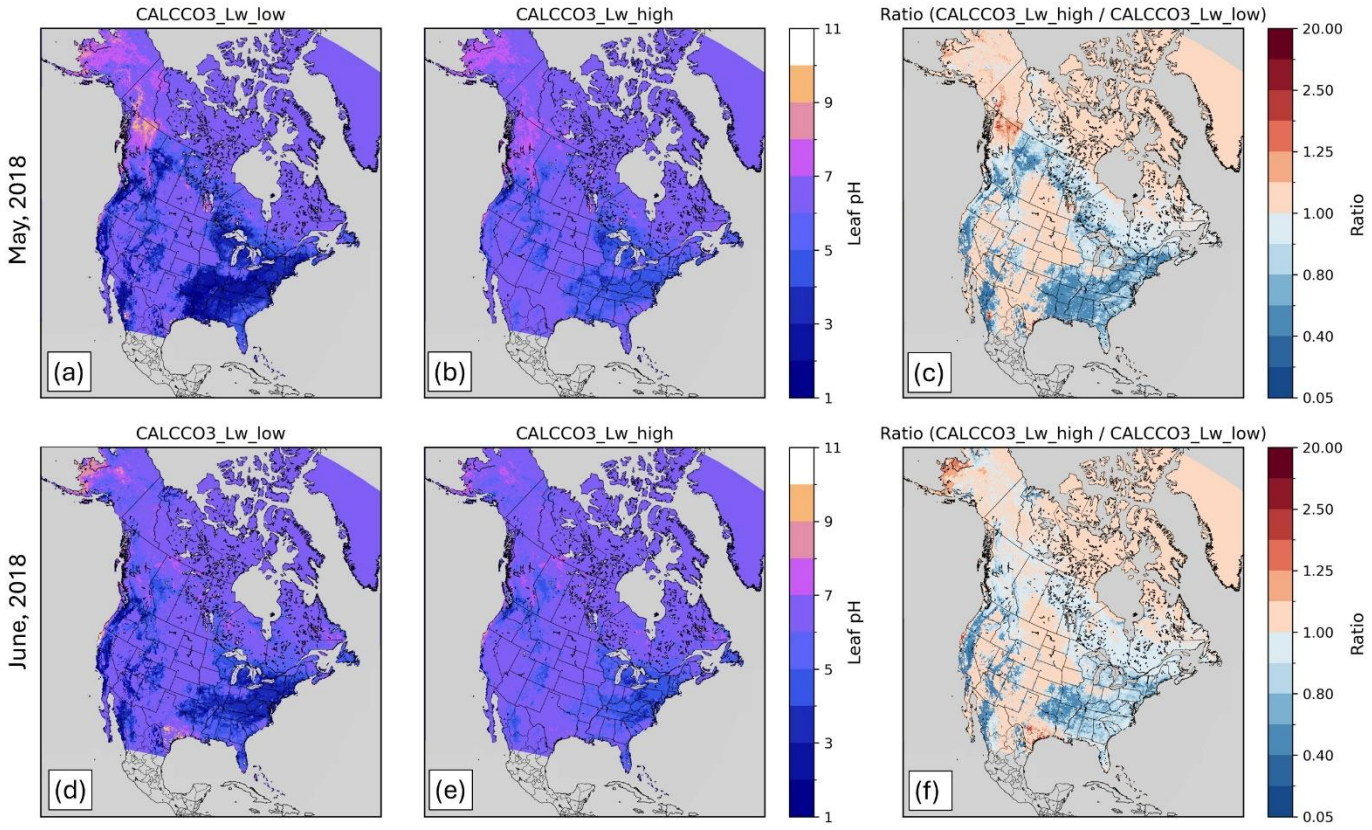

Please remove the "(Case #2)" here. That's from the ACPD version of the text.

Figure S2: The mean monthly pH predicted for May 2018 (a – c) and June 2018 (d – f) using the low and high Lw thresholds.

The first column (a, d) shows the mean pH predicted by CALCCO3_Lw_low and the second column (b, e) by CALCCO3_Lw_high (Case #2). The third column shows the ratio of the results from the two model runs, calculated as CALCCO3_Lw_high / CALCCO3_Lw_low, demonstrating the impact of the choice of low leaf water thickness threshold on the calculated pH. In the ratio plots (c,f), red colours denote areas where the predicted pH is greater in CALCCO3_Lw_low than CALCCO3_Lw_high, and vice versa for blue colours. Grey regions indicate water bodies or areas outside the 10km model domain (such as southern Mexico, northern Greenland). In both configurations, when $\boldsymbol{L_w} < \boldsymbol{L_{wThres}}$, the pH is assumed to be 6.68.

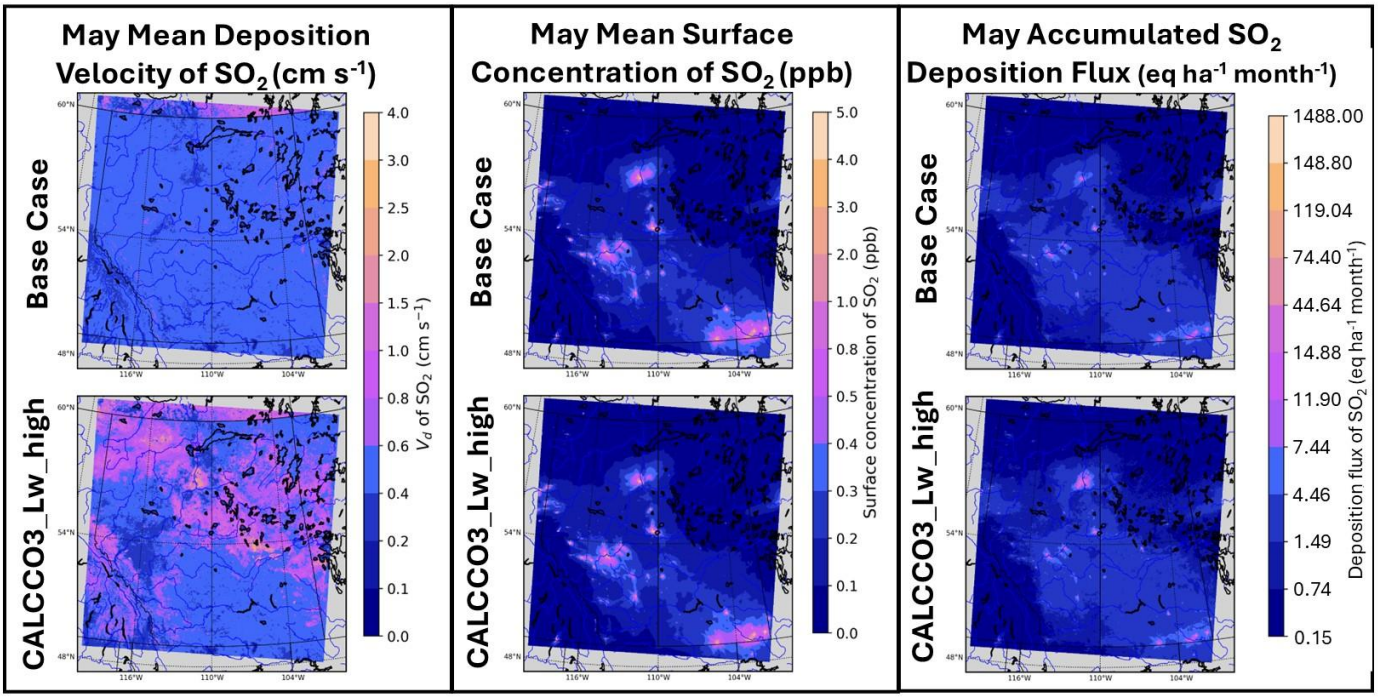

Figure S3: May mean $V_{d_{SO_2}}$ (cm s^{-1}), mean surface SO_2 concentration (ppb), and monthly accumulated deposition flux (eq ha^{-1} $month^{-1}$), for the Base Case and CALCCO3_Lw_high simulations. Note that equivalents correspond to units of moles x charge, and 2 negative charges are assumed for every mole of SO_2 deposition.

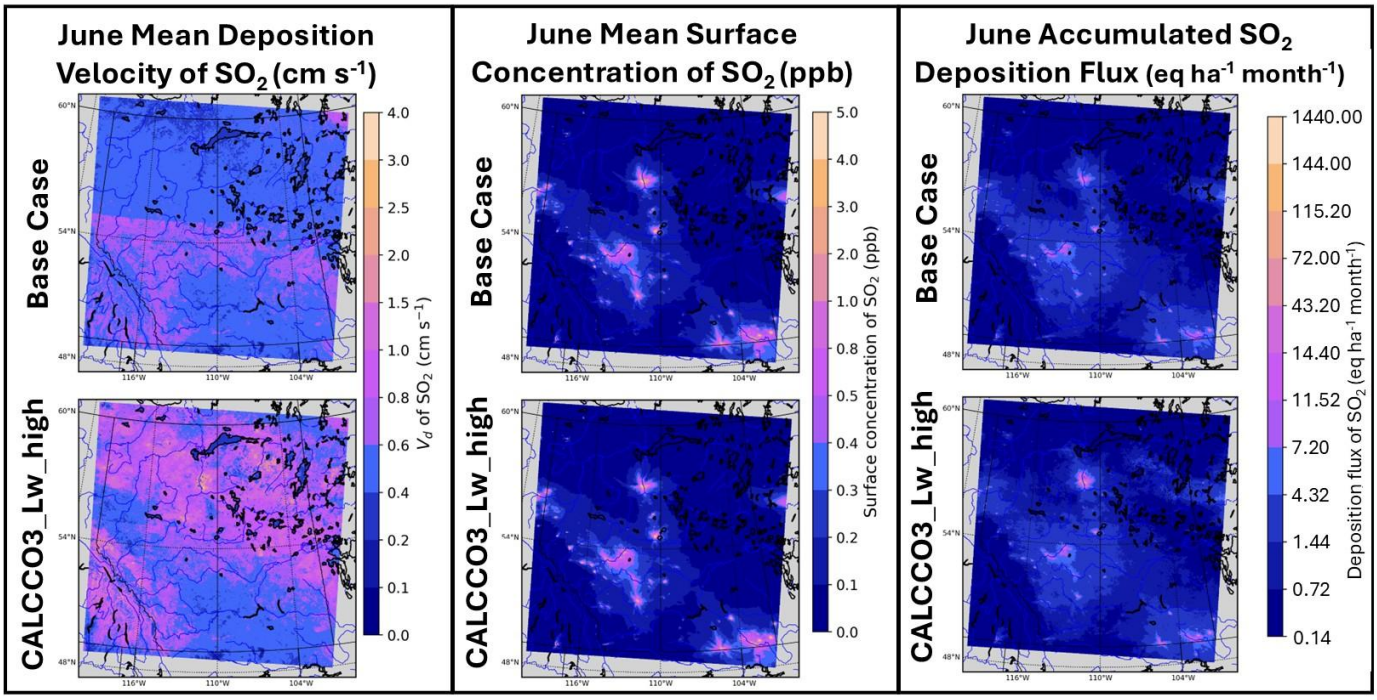

Figure S4: June mean $V_{d_{SO_2}}$ (cm s^{-1}), mean surface SO_2 concentration (ppb), and monthly accumulated deposition flux (eq ha^{-1} $month^{-1}$), for the Base Case and CALCCO3_Lw_high simulations.

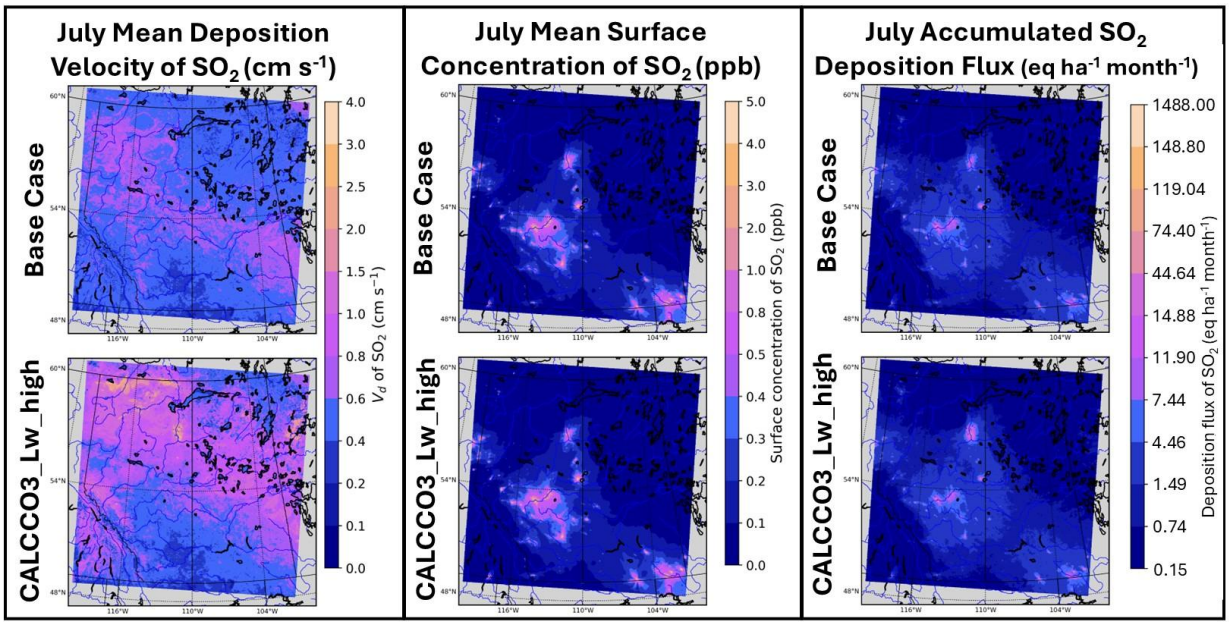

Figure S5: July mean $V_{d_{SO_2}}$ (cm s^{-1}), mean surface SO$_2$ concentration (ppb), and monthly accumulated deposition flux (eq ha^{-1} month^{-1}), for the Base Case and CALCCO3_Lw_high simulations.

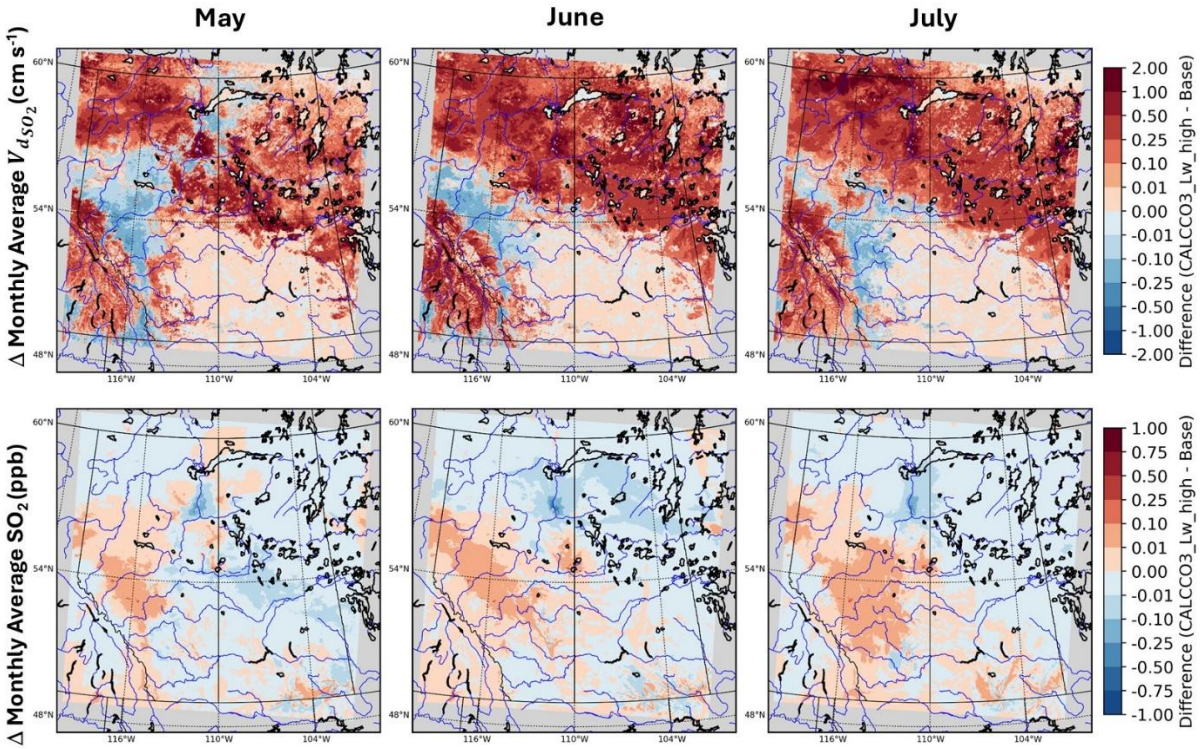

Figure S6: Differences between monthly averages (CALCCO3_Lw_high – Base Case) for monthly average $V_{d_{SO_2}}$ (cm s^{-1}) (top row), and surface SO$_2$ concentration (ppbv) (bottom row).

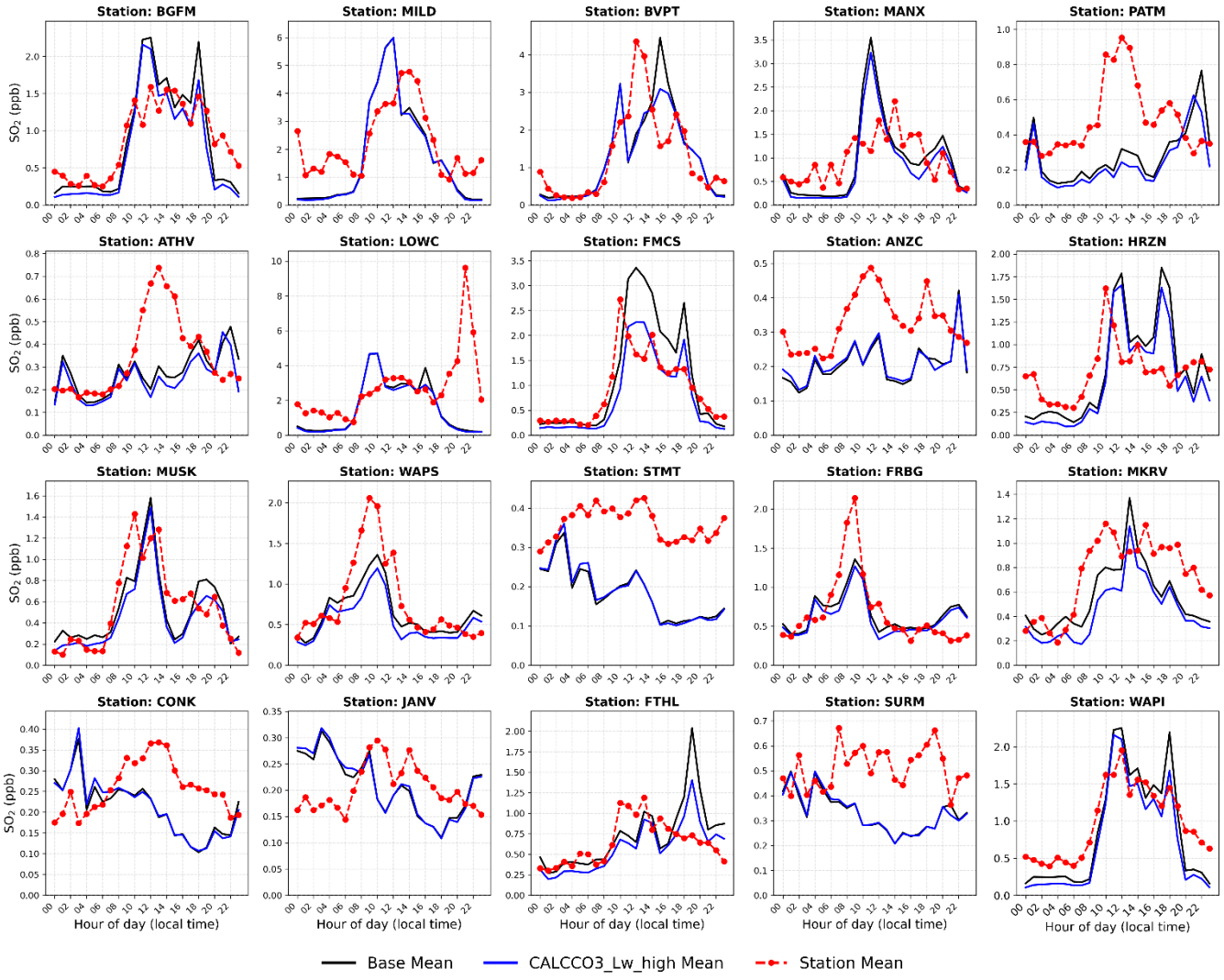

Figure S7: Identical to Fig. 10 except now for May 2018. Also shown in each plot is the surface SO_2 concentration predicted by CALCCO3_Lw_low (orange line).

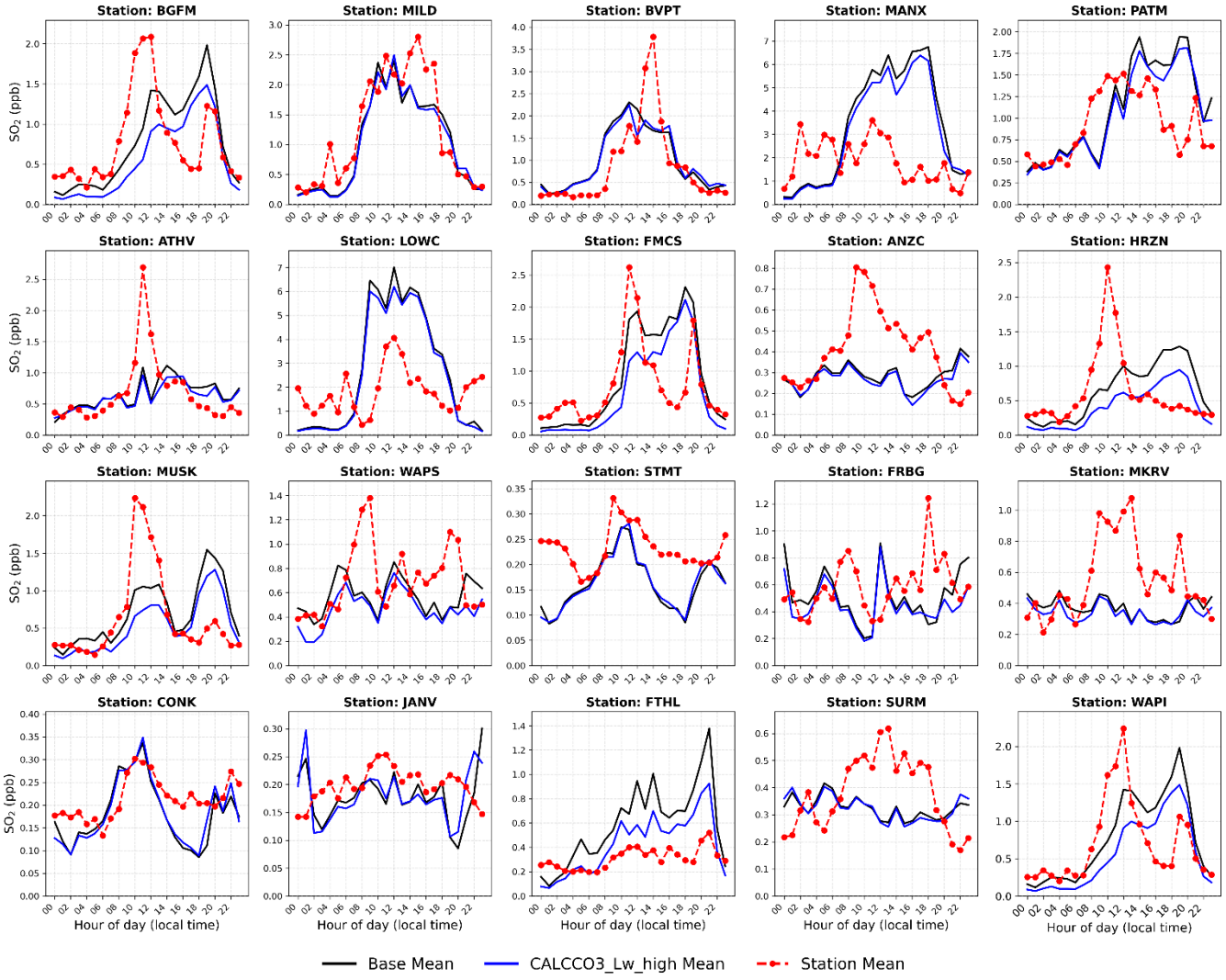

Figure S8: Identical to Fig. 10 except now for July 2018. Also shown in each plot is the surface SO_2 concentration predicted by CALCCO3_Lw_low (orange line).

340

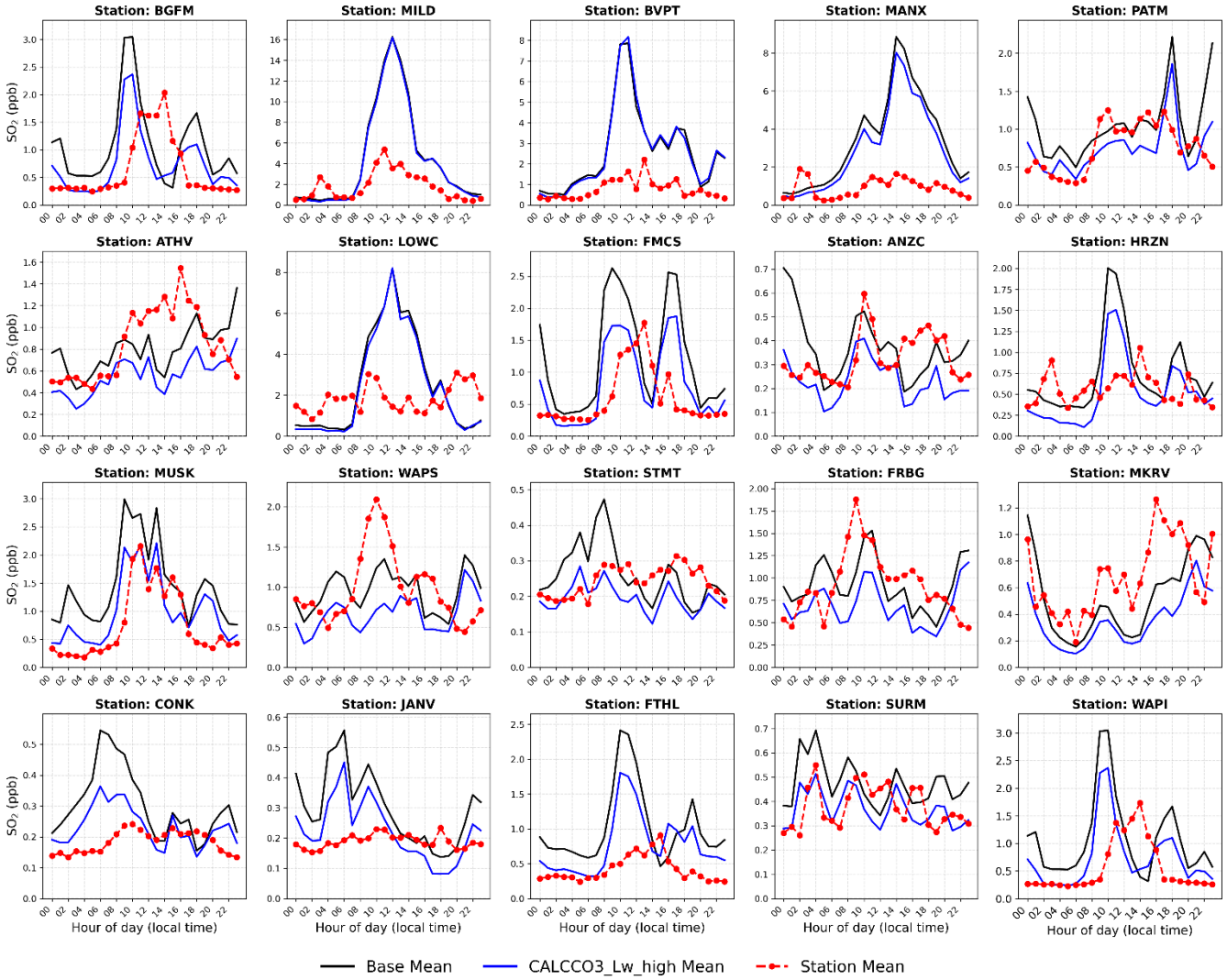

Please change this to "Fig. 10 in the main text, except now for August 2018".

Figure S9: Identical to Fig. 10 except now for August 2018.

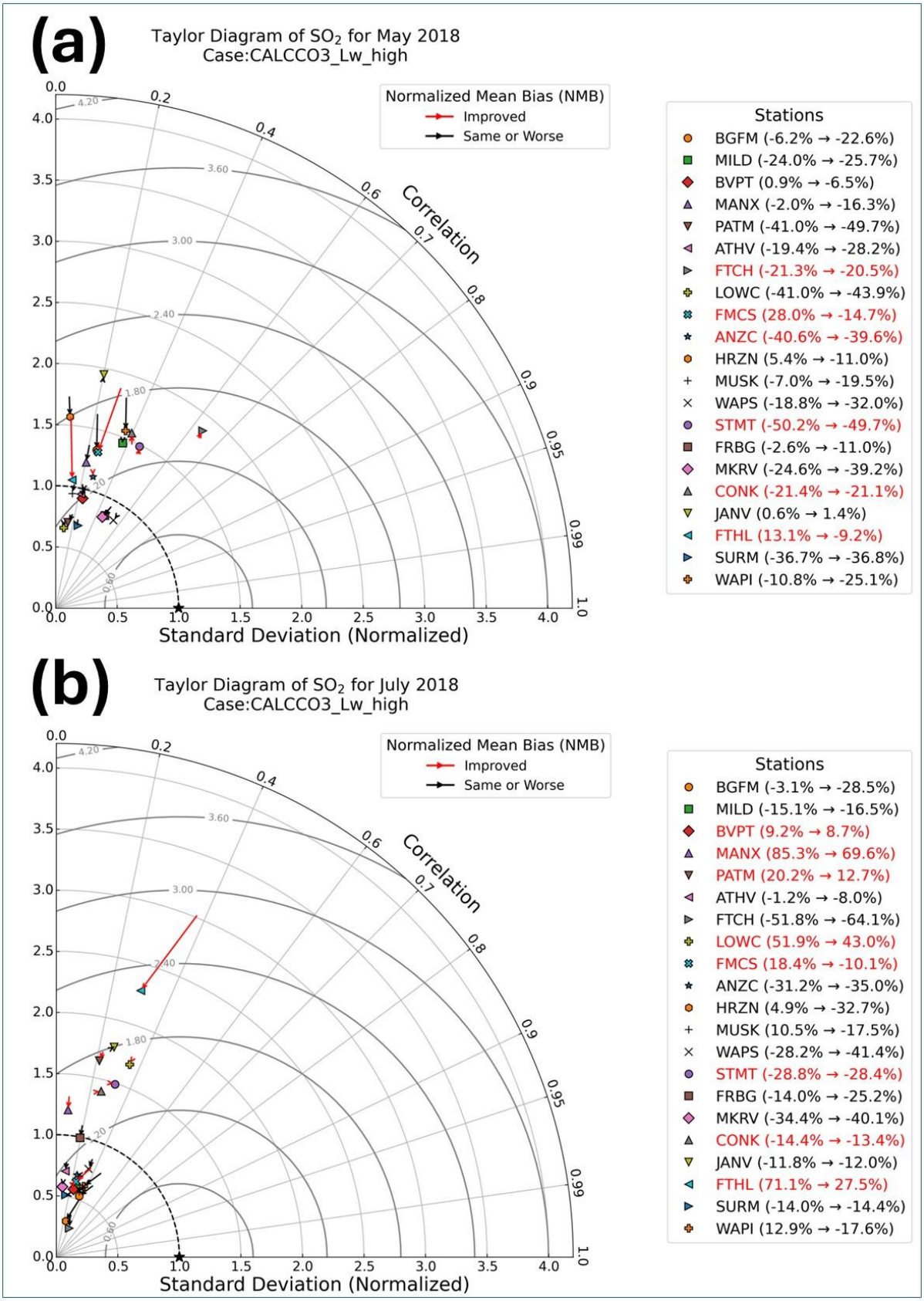

345 **Figure S10: Identical to Fig. 11 except now for May (a) and July (b) of 2018.**

Table S4: Formulae used to perform statistical evaluation of the modelled SO_2 surface concentrations compared to observations.

Variable (Abbreviation)	Formulae	Definition	Ideal score
n	-	Number of hourly model-observation pairs used in the evaluation	-
o_i	-	Observed value at time i	-
m_i	-	Modelled value at time i	-
$\bar{o}$	$\bar{o} = \frac{1}{n}\sum_{i=1}^{n} o_i$	Average (mean) of the observed values.	-
$\bar{m}$	$\bar{m} = \frac{1}{n}\sum_{i=1}^{n} m_i$	Average (mean) of of the modelled values.	$\bar{m} = \bar{o}$
σ_O	$\sigma_o = \left(\frac{\sum_{i=1}^{n}(o_i - \bar{o})}{n-1}\right)^{\frac{1}{2}}$	Sample standard deviation of the observed values.	-
σ_m	$\sigma_m = \left(\frac{\sum_{i=1}^{n}(m_i - \bar{m})}{n-1}\right)^{\frac{1}{2}}$	Sample standard deviation of the modelled values.	$\sigma_m = \sigma_o$
NSD	$\mathrm{NSD} = \frac{\sigma_m}{\sigma_O}$	Normalized standard deviation (NSD). The standard deviation of the model normalized by the standard deviation of the observations.	NSD = 1.0
r	$r = \frac{1}{n-1}\sum_{i=1}^{n}\left[\left(\frac{m_i - \bar{m}}{\sigma_m}\right)\left(\frac{o_i - \bar{o}}{\sigma_O}\right)\right]$	The Pearson correlation coefficient which describes the degree of linear dependence between the modelled and observed values.	$r = 1.0$
NMB	$\mathrm{NMB} = \frac{\sum_{i=1}^{n}(m_i - o_i)}{\sum_{i=1}^{n} o_i} \times 100\ \%$	Normalized mean bias (NMB), representing the average of the difference (model minus observation) for all data pairs normalized by the average of the observations. Negative (positive) values indicate the model value is lower (greater) than the observations. Expressed as a percentage.	NMB = 0.0 %
RMSE	$\mathrm{RMSE} = \left[\frac{\sum_{i=1}^{n}(m_i - o_i)}{n}\right]^{\frac{1}{2}}$	Root-mean square error (RMSE), representing the standard deviation of differences between the model and observations.	RMSE = 0.0
NRMSE	$\mathrm{NRMSE} = \frac{\mathrm{RMSE}}{\bar{o}} \times 100\ \%$	Normalized root-mean square error (NRMSE). The RMSE normalized by the average of the observations. Expressed as a percentage.	NRMSE = 0.0 %
MAE	$\mathrm{MAE} = \frac{1}{n}\sum_{i=1}^{n}\lvert m_i - o_i\rvert$	Mean absolute error (MAE).	MAE = 0.0 %
NMAE	$\mathrm{NMAE} = \frac{1}{n}\sum_{i=1}^{n}\frac{\lvert m_i - o_i\rvert}{o_i}$	Normalized mean absolute error (NMAE).	NMAE = 0.0 %
IOA	$\mathrm{IOA} = 1.0 - \frac{\sum_{i=1}^{n}\lvert m_i - o_i\rvert}{2\sum_{i=1}^{n}\lvert o_i - \bar{o}\rvert}$	Index of agreement (IOA).	IOA = 1.0

350

S6.0 References, Supplemental Material

Chameides, W. L.: The photochemistry of a Remote Marine Stratiform Cloud, J. Geophys. Res.: Atm., 89(D3), 4739–4755, https://doi.org/10.1029/jd089id03p04739, 1984.

Clifton, O. E., Schwede, D., Hogrefe, C., Bash, J. O., Bland, S., Cheung, P., Coyle, M., Emberson, L., Flemming, J., Fredj, E., Galmarini, S., Ganzeveld, L., Gazetas, O., Goded, I., Holmes, C. D., Horváth, L., Huijnen, V., Li, Q., Makar, P. A., Mammarella, I., Manca, G., J. Munger, J.W., Pérez-Camanyo, J.L., Pleim, J., Ran, L., San Jose, R., Silva, S. J., Staebler, R., Sun, S., Tai, A. P. K., Tas, E., Vesala, T., Weidinger, T., Wu, Z. and Zhang, L.: A single-point modeling approach for the Intercomparison and evaluation of ozone dry deposition across chemical transport models (activity 2 of AQMEII4), Atmos. Chem. Phys., 23(17), 9911–9961, https://doi.org/10.5194/acp-23-9911-2023, 2023.

Emerson, E. W., Hodshire, A. L., DeBolt, H. M., Bilsback, K. R., Pierce, J. R., McMeeking, G. R., and Farmer, D. K.: Revisiting particle dry deposition and its role in radiative effect estimates, Proc. Natl. Acad. Sci. U.S.A., 117(42), 26076–26082, https://doi.org/10.1073/pnas.2014761117, 2020.

Ervens, B., George, C., Williams, J. E., Buxton, G. V., Salmon, G. A., Bydder, M., Wilkinson, F., Dentener, F., Mirabel, P., Wolke, R. and Herrmann, H.: CAPRAM 2.4 (MODAC mechanism): An extended and condensed tropospheric aqueous phase mechanism and its application, J. Geophys. Res.: Atm., 108(D14), https://doi.org/10.1029/2002jd002202, 2003.

Fountoukis, C. and Nenes, A.: ISORROPIA II: A computationally efficient thermodynamic equilibrium model for K^+–Ca^{2+}–Mg^{2+}–NH_4^+–Na^+–SO_4^{2-}–NO_3^-–Cl^-–H_2O aerosols, Atmos. Chem. Phys., 7(17), 4639–4659, https://doi.org/10.5194/acp-7-4639-2007, 2007.

Galmarini, S., Makar, P., Clifton, O. E., Hogrefe, C., Bash, J. O., Bellasio, R., Bianconi, R., Bieser, J., Butler, T., Ducker, J., Flemming, J., Hodzic, A., Holmes, C. D., Kioutsioukis, I., Kranenburg, R., Lupascu, A., Perez-Camanyo, J. L., Pleim, J., Ryu, Y.-H., San Jose, R., Schwede, D., Silva, S. and Wolke, R.: Technical note: AQMEII4 activity 1: Evaluation of wet and dry deposition schemes as an integral part of regional-scale air quality models, Atmos. Chem. Phys., 21(20), 15663–15697, https://doi.org/10.5194/acp-21-15663-2021, 2021.

Makar, P. A., Akingunola, A., Aherne, J., Cole, A. S., Aklilu, Y.-A., Zhang, J., Wong, I., Hayden, K., Li, S.-M., Kirk, J., Scott, K., Moran, M. D., Robichaud, A., Cathcart, H., Baratzedah, P., Pabla, B., Cheung, P., Zheng, Q., and Jeffries, D. S.: Estimates of exceedances of critical loads for acidifying deposition in Alberta and Saskatchewan, Atmos. Chem. Phys., 18, 9897–9927, https://doi.org/10.5194/acp-18-9897-2018, 2018.

Meng, Z., Seinfeld, J. H., Saxena, P. and Kim, Y. P.: Atmospheric gas-aerosol equilibrium: IV. thermodynamics of carbonates, Aerosol Sci. Technol., 23(2), 131–154, https://doi.org/10.1080/02786829508965300, 1995.

Shi, Q., Davidovits, P., Jayne, J. T., Worsnop, D. R. and Kolb, C. E.: Uptake of gas-phase ammonia. 1. Uptake by aqueous surfaces as a function of pH, J. Phys. Chem. A., 103(44), 8812–8823, https://doi.org/10.1021/jp991696p, 1999.

Toyota, K., Makar, P. A., Savic-Jovcic, V., Robichaud, A., Lupu, A., Chen, J., Clifton, O.E., Hogrefe, C., and Galmarini, S.: Performance of surface ozone prediction by the regional air-quality model GEM-MACH: Sensitivities to dry deposition and canopy effects on chemistry and diffusion, in preparation, 2026.

Wesely, M.: Parameterization of surface resistances to gaseous dry deposition in regional-scale numerical models, Atmos. Environ., 23, 1293–1304, https://doi.org/10.1016/0004-6981(89)90153-4, 1989.

Zhang, L., Gong, S., Padro, J. and Barrie, L.: A size-segregated particle dry deposition scheme for an atmospheric aerosol module, Atmos. Environ., 35, 549–560, https://doi.org/10.1016/S1352-2310(00)00326-5, 2001.

Zhang, L., Moran, M. D., Makar, P. A., Brook, J. R. and Gong, S.: Modelling gaseous dry deposition in AURAMS: a unified re gional air-quality modelling system, Atmos. Environ., 36, 537-560, https://doi.org/10.1016/S1352-2310(01)00447-2, 2002.

Zhang, L., Brook, J. R., and Vet, R.: A revised parameterization for gaseous dry deposition in air-quality models, Atmos. Chem. Phys., 3, 2067–2082, https://doi.org/10.5194/acp-3-2067-2003, 2003.

Zhang, L., Wright, L. P. and Asman, W. A.: Bi-directional air-surface exchange of atmospheric ammonia: A review of measurements and a development of a big-leaf model for applications in regional-scale air-quality models, J. Geophys. Res.: Atm., 115(D20), https://doi.org/10.1029/2009jd013589, 2010.